International Journal of Concrete Structures and Materials

RESEARCH Open Access

Numerical Analysis of Shear Contribution of CFRP-Strengthened RC Beams by Different Bond-Slip Models

Shengqiang Ma[1,2*], Jianfeng Sun[2] and Tiancai Xu[2]

Abstract

During a numerical investigation conducted using ABAQUS software, various bond-slip models for the FRP–concrete interface were evaluated to accurately predict the shear contribution of FRP in strengthening reinforced concrete (RC) beams. Three established bond-slip models were chosen to develop finite element analysis models for the four FRP-strengthened beams. The outcomes of these numerical simulations were subsequently compared with experimental data. The results demonstrated a strong correlation between the finite element simulations and the experimental tests, particularly regarding the failure process and shear capacity of the reinforced beams. The increase in shear capacity observed during testing varied from 13.5% to 42.9%. In contrast, the corresponding increase in shear capacity predicted by the finite element simulations ranged from 5.5% to 47.7%. The discrepancy in CFRP shear contribution among beams with different bond-slip relationships, under identical reinforcement configurations, was observed to be within the range of 0.1% to 15.9%. The numerical results of the Nakaba model showed a higher level of safety; however, the simulation performance of the Lu model was regarded as more effective and better suited for numerical analysis in predicting the shear contribution of FRP in strengthened RC beams.

Keywords Reinforced concrete beam, CFRP shear reinforcement, Numerical analysis, FRP–concrete interface, Bond-slip model

1 Introduction

Over the past three decades, there has been an increasing application of fiber-reinforced polymers (FRPs) in the rehabilitation of reinforced concrete (RC) structures, significantly enhancing the load-bearing capacity of structural components (Haddad et al., 2013; Junaid et al., 2022; Al Shboul et al.,2024). This trend is attributed to the outstanding properties of FRPs, including lightweight, high tensile strength, corrosion resistance, and ease of fabrication.

To date, a plethora of experimental and theoretical studies have been conducted to investigate the flexural and shear capacity of FRP-strengthened RC beams (Askar and Abd-Alkhalek, 2012; Dong et al., 2013; Moradi et al., 2020; Sayed et al., 2014; Zhou et al., 2019). The results of these research efforts have been extensively documented.

Typically, RC structures are strengthened by immersing continuous fibers in a resin matrix, which is subsequently bonded to the surface of the structures. For flexural strengthening, FRP sheets are affixed to the bottom of beams along the longitudinal directions. In contrast, for shear strengthening, FRP sheets are employed to impede the progression of shear cracks and enhance the shear resistance of RC beams through three distinct

*Correspondence:
Shengqiang Ma
msq-2000@163.com
[1] Key Laboratory of Transport Industry of Bridge Detection Reinforcement Technology, Chang'an University, Xi'an, China
[2] School of Architecture and Engineering, Xinjiang University, Ürümqi, Xinjiang 830047, China

strengthening schemes: full wrapping (FW), U-jacket (U), and side bonding (S) (Ma et al., 2019).

The bond between the FRP sheets and the concrete surface is crucial for transferring the FRP's strength to the structure and significantly impacts the behavior of retrofitted beams. The performance of the FRP–concrete interface is vital for ensuring effective interaction between the two materials. Since the FRP–concrete interface plays a direct role in stress transfer efficiency, any occurrence of debonding can substantially compromise the performance of FRP-strengthened beams (Teng et al., 2003).

As a result, the techniques of anchoring grooves and holes were employed to enhance the bond between concrete and CFRP, thereby significantly improving the bond-slip behavior of concrete beams with CFRP composites (Al-Rousan and Abu-Elhija,2020; Al-Rousan and AL-Tahat, 2020a,2020b; Haddad and Al-Rousan, 2016). Nevertheless, there has been limited focus on developing models to characterize the bond-slip relationship in FRP-strengthened beams (Augusthus Nelson et al., 2020; Li et al., 2018; Lin & Zhang, 2013). However, capturing macroscopic changes at the interface during the FRP reinforcement of RC beams presents significant challenges in experimental setups. Additionally, the high costs and difficulties in controlling experimental errors highlight the necessity for alternative approaches (Jahangir and Esfahani, 2018). With the rapid advancements in computer hardware and software, simulating actual tests using finite element software offers a more cost-effective and efficient approach to investigating interface changes. The bond-slip model of the FRP–concrete interface is crucial for the numerical analysis of shear contributions from FRP. Therefore, conducting in-depth research on the bond-slip behavior of the FRP–concrete interface and developing an accurate and reliable constitutive model is essential for the mechanical analysis of FRP-strengthened beams.

In the realm of research on FRP shear-strengthened RC rectangular section beams, numerous experimental and theoretical studies have been undertaken (Tahir et al., 2019; Phan-Vu et al., 2021; Al-Allaf et al., 2019). Besides, researchers tried to conduct the experiment from pull-out tests to develop empirical models to modify the bond-slip behavior between concrete and CFRP (Alhassan et al.,2019; Haddad et al.,2015; Al-Rousan et al.,2015). However, there has been a relative scarcity of research among scholars regarding the application of the bond-slip relationship in finite element simulations. (Lee et al., 2017; Lee and Al-Mahaidi, 2008; Alhassan et al., 2020). Furthermore, some researchers have developed various bond-slip models to characterize the mechanical behavior of the interface by applying regression and fitting techniques to in-plane shear test data (Kasumassa Nakaba and Hiroyuki, 2001; Lin & Zhang, 2013; Lu et al., 2005; Monti et al., 2003).

The significant influence of the FRP–concrete interface bonding on reinforcement effectiveness, as evidenced by existing research findings, highlights the necessity for a thorough investigation of the bond-slip relationship within the FRP–concrete interface. The primary objective of this study is to simulate the shear reinforcement effects arising from established bond-slip relationships in FRP shear-strengthened RC beams. By comparing these simulations with experimental results, the three common bond-slip models are compared and evaluated to find the most suitable model for future numerical analysis of the shear contribution of RC beams reinforced with FRP.

2 Experimental Investigation

To investigate the contribution of FRP shear in shear-strengthened beams, four distinct strengthening techniques were implemented for the RC beams: discrete side bonding (SS), discrete U jacketing (SU), continuous side bonding (CS), and continuous U jacketing (CU). This study offers reliable test data applicable to these four shear reinforcement methods in both finite element simulations and practical engineering applications. To induce shear failure in the beams, the specimens were designed with a higher ratio of tensile reinforcement and a reduced ratio of stirrup reinforcement.

2.1 Specimen Design and Material

In this study, a total of five beams were cast for shear testing, comprising one control beam and four carbon fiber-reinforced polymer (CFRP) strengthened reinforced concrete (RC) beams, all featuring rectangular cross-sections. The dimensions of the test specimens were 1500 mm in length, 150 mm in width, and 260 mm in height. The section dimension and reinforcement configuration of the beams are depicted in Fig. 1. C45-grade concrete was utilized to achieve the targeted strength for the beams in accordance with Chinese standards (JTG 3362–2018). The compressive strength of the concrete cubes, measured after 28 days of curing and with dimensions of 150×150×150 mm, was 47.8 MPa. For the longitudinal reinforcement designed to bear the bending moment, HRB400 steel with a diameter of 22 mm was utilized. Additionally, HPB300 steel with a diameter of 6 mm was employed for stirrup reinforcement, spaced at 200 mm to effectively resist shear, resulting in a reinforcement ratio of 0.189. Both types of steel comply with Chinese standards (JTG 3362–2018). The yield strength, ultimate strength, and elastic modulus of the steel reinforcement are detailed in Table 1.

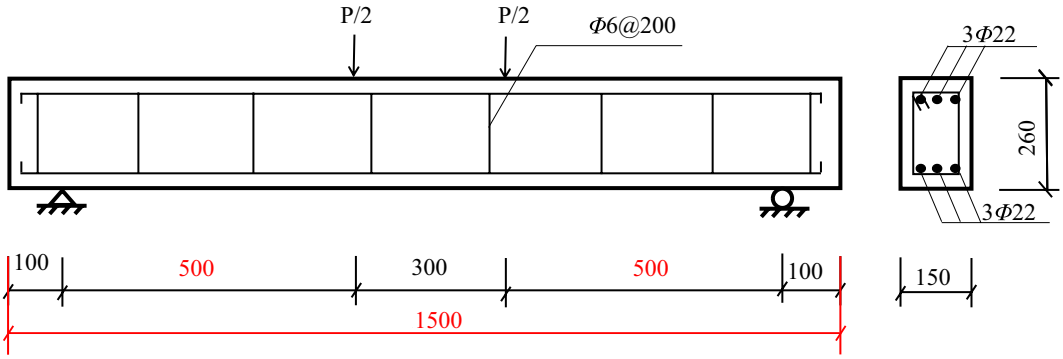

Fig. 1 Dimension of beam and arrangement of reinforcement (unit: mm)

Table 1 Mechanical properties of materials

Material	Type	Yield strength/MPa	Ultimate strength/MPa	Elastic modulus/GPa
HPB300	Φ6	345	447	210
HRB400	Φ22	416	510	210
–	CFRP	–	3480	250
C45	Concrete	–	47.8	–

The CFRP sheets applied to the beams had a thickness of 0.167 mm and exhibited a tensile strength of 3480 MPa. The material properties of the CFRP sheets are provided in Table 1.

2.2 Strengthened Scheme

In the study, one beam served as the control specimen, labeled "B1". The remaining four beams were reinforced using four distinct configurations of CFRP. Specifically, "B-SS" and "B-SU" refer to beams reinforced with discrete side bonding and U-jacketing, respectively, with a width of 50 mm and a spacing of 100 mm. Conversely, "B-CS" and "B-CU" represent beams strengthened with continuous side bonding and U-jacketing, respectively. The reinforcement schemes for each specimen are visually illustrated in Fig. 2.

2.3 Test Setup and Instrument

All specimens were subjected to testing using the four-point bending method. The MAS-500 servo-hydraulic testing machine was utilized to apply a two-point load on the top of the beams through the distribution beam. Two supporting pins conveyed equal forces to the beam, strategically positioned 150 mm from the center of the beam. During the testing process, the progression of cracks was carefully marked, and data were systematically recorded for the mid-span deflection of the concrete beam, CFRP strain, and the applied load. In order to capture shear phenomena and the bond-slip behavior between CFRP and concrete, strain gauges were thoughtfully installed on the surface of the CFRP sheets along the diagonal direction of the beam. The precise positioning of the strain gauges and linear variable displacement transducers (LVDTs) is represented in Fig. 3.

3 Numerical Modeling

3.1 Material Constitutive Relation

In this study, the constitutive relation of concrete employed in the numerical simulation was derived from the literature (Ding et al., 2010). This constitutive model is characterized by a continuous variation law that is applicable to all concrete grades, and it offers a simple formulation along with high computational accuracy (Ding et al., 2011). The equation for the full stress–strain curve under compression is calculated as follows:

$$y = \begin{cases} \frac{A_1 x - x^2}{1+(A_1-2)x} & x \le 1 \\ \alpha_1 (x-1)^2 + x & x > 1 \end{cases}, \quad (1)$$

where $y = \sigma / f_c$; $x = \varepsilon / \varepsilon_c$; f_c is the axial compressive strength, $f_c = 0.4 f_{cu}^{7/6}$; the parameter of the ascending segment of the curve is taken: $A_1 = 9.1 f_{cu}^{-4/9}$; the parameter of the descending segment of the curve is taken: $\alpha_1 = 2.5 \times 10^{-5} f_{cu}^3$; f_{cu} is the ultimate compressive strength of concrete cube.

Equation of the full stress–strain curve under tensile is calculated as follows:

$$y = \begin{cases} \frac{A_2 X - X^2}{1 + (A_2 - 2)X} & X \le 1 \\ \alpha_2 (X - 1)^{1.7} + X & X > 1 \end{cases} \quad (2)$$

where $y = \sigma / f_t$; $x = \varepsilon / \varepsilon_c$; f_t is the axial tensile strength, $f_t = 0.24 f_{cu}^{2/3}$; the parameter of the ascending segment of the curve is taken: $A_2 = 1.306$; the parameter of the descending segment of the curve is taken: $\alpha_2 = 1 + 3.4 \times 10^{-4} f_{cu}^2$.

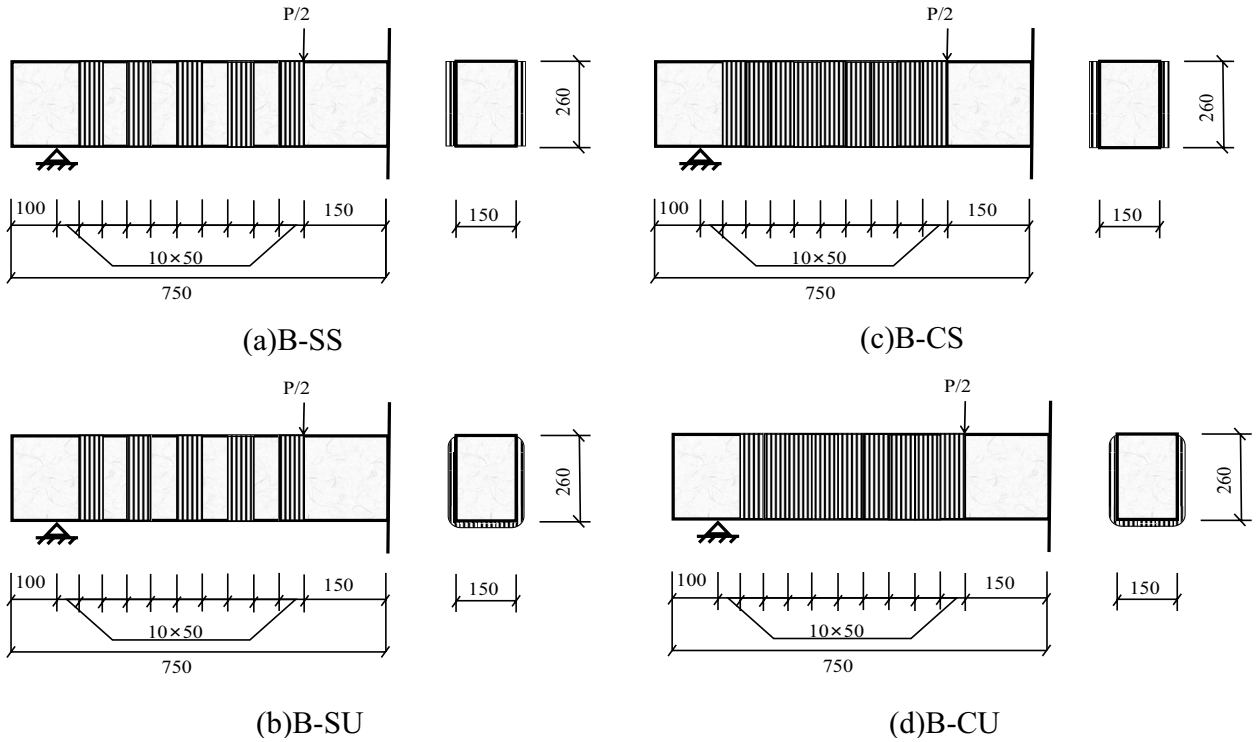

Fig. 2 CFRP strengthening configurations

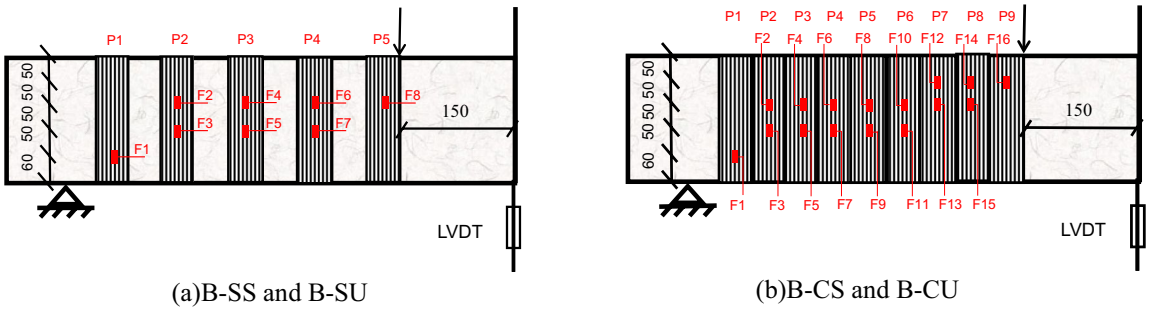

Fig. 3 Test setup and instrument installation

Considering the good convergence performance of the model and the requirement of simulation accuracy, the ideal elastic–plastic model was selected as the constitutive equations of reinforcement material, and the linear elastic model was selected as the constitutive equations of CFRP material.

3.2 Interface of FRP–Concrete Constitutive

The cohesion model was utilized to investigate the mechanical behavior of the interface between CFRP and concrete. This model effectively simulates the complex failure mechanisms that occur between the two surfaces by establishing a stress–slip relationship. To establish the stress–slip relationship of the cohesion model, it is essential to determine the maximum stress in the three directions of the simulated material. The key parameters include the slip corresponding to the maximum stress, the maximum slip s_u, the initial stiffness k_0, and the softening stiffness k, as illustrated in Fig. 4. The constitutive relation is expressed as follows:

$$\begin{Bmatrix} \tau_n \\ \tau_s \\ \tau_t \end{Bmatrix} = \begin{Bmatrix} K_{nn} & & \\ & K_{ss} & \\ & & K_{tt} \end{Bmatrix} \begin{Bmatrix} \varepsilon_n \\ \varepsilon_s \\ \varepsilon_t \end{Bmatrix}, \tag{3}$$

where $\tau_i (i = n, s, t)$ is the stress in three directions on the interface; $K_{ii} (i = n, s, t)$ is the stiffness coefficient

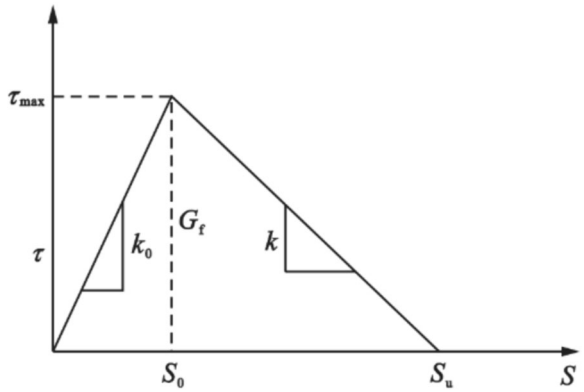

Fig. 4 Constitutive relation of CFRP–concrete interface

corresponding to the normal stress and two shear stress on the interface; $\varepsilon_i (i = n, s, t)$ is the strain in three directions on the interface.

As the FRP–concrete interface initiates stress, the shear stresses in three directions on the interface undergo an elastic stage where stress increases with deformation. Upon reaching the peak value, damage to the interface begins, transitioning into the softening stage, leading to a reduction in bond stiffness. Ultimately, upon failure, the shear stress drops to zero, and the relative deformation reaches its maximum. The energy consumed throughout this process represents the maximum fracture energy (G_f), quantified by the area enclosed by the stress–separation relation curve of the interface and the coordinate axes.

Currently, numerous scholars have proposed various models to describe the bond-slip relationships at the FRP–concrete interface. In this research, three specific bond-slip relationships were selected as the constitutive models for the CFRP–concrete interface in the finite element modeling of four reinforced concrete beams. These relationships are as follows:

(1)(1)(1)(1) Nakaba model (Nakaba et al. 2001).

Nakaba et al. (2001) utilized the differential interpolation method to regress the bilinear model based on strain data collected from 30 in-plane shear tests:

$$\tau = \tau_{\max}\left[\frac{s}{s_0}\frac{3}{2+(s/s_0)^3}\right], \tag{4}$$

$$\tau_{\max} = 3.5\, f_c^{0.19}. \tag{5}$$

Based on above model, the parameters of all CFRP-strengthened beams in this research were calculated as: $s_0 = 0.065$ mm;τ_{max}=7.29 MPa; s_u=0.5 mm; k_0=106.6 MPa/mm; G_f=1.98N/mm.

(2) Monti model (Monti et al., 2003).

Monti et al. (Monti et al., 2003) considered the elastic modulus and width correction coefficient of the adhesive layer. They utilized the differential interpolation method to obtain data from in-plane shear tests and fitted a bilinear model suitable for the peeling test:

$$\tau = \begin{cases} \tau_{\max}\left(\frac{s}{s_0}\right) & s \le s_0 \\ \tau_{\max}\left(\frac{s_u - s}{s_u - s_0}\right) & s_0 < s \le s_u \\ 0 & s > s_u \end{cases}, \tag{6}$$

$$\tau_{\max} = 1.8\beta_w f_t, \tag{7}$$

$$s_0 = 2.5\tau_{\max}\left(\frac{t_a}{E_a} + \frac{50}{E_c}\right), \tag{8}$$

$$s_u = 0.33\beta_w, \tag{9}$$

$$\beta_w = \sqrt{\frac{1.5(2 - b_f/b_c)}{1 + b_f/100}}, \tag{10}$$

where E_a and t_a are the elastic modulus and thickness of the adhesive layer, respectively; E_C is the elastic modulus of concrete; b_f and b_c are FRP strip width and concrete width, respectively; β_w is the width correction coefficient.

Based on above model, the parameters of B-SS and B-SU beams with the discrete strips were figured out as τ_{max}=6.97 MPa, s_0=0.032 mm, s_u=0.4 mm,k_0=221.3 MPa/mm, and G_f=1.39N/mm; the parameters of continue strips strengthened beams B-CS and B-CU were as τ_{max}=5.69 MPa,s_0=0.026 mm,s_u=0.33 mm,k_0=218.8 MPa/mm, and G_f=0.93N/mm.

(3) Lu model (Lu et al., 2005).

Lu et al. (2005) developed a refined model utilizing finite element software to simulate and analyze the strain–slip characteristics at the FRP–concrete interface during the failure process, obtaining an accurate model through analysis. Initially, the model was simplified by considering the negligible impact of the adhesive layer stiffness on the failure energy of the interface. The results indicated that maintaining the total failure energy and the coordinates of the maximum interfacial shear force point (τ_{max},s_0) unchanged allowed for further simplification of the model into a bilinear model:

$$\tau = \begin{cases} \tau_{\max}\left(\frac{s}{s_0}\right) & s \le s_0 \\ \tau_{\max}\left(\frac{s_u - s}{s_u - s_0}\right) & s_0 < s \le s_u \\ 0 & s > s_u \end{cases}, \tag{11}$$

$$\tau_{\max} = 1.5\beta_w f_t, \tag{12}$$

$$s_0 = 0.0195\beta_w f_t, \tag{13}$$

$$s_u = 2G_f/\tau_{\max}, \tag{14}$$

$$\beta_w = \sqrt{\frac{2.25 - b_f/b_c}{1.25 + b_f/b_c}}, \tag{15}$$

$$G_f = 0.308\beta_w^2\sqrt{f_t}. \tag{16}$$

According to the above model, the parameters of the discrete strips strengthened beams B-SS and B-SU were calculated as: $\tau_{\max}=4.74$ MPa,$s_0=0.06$ mm,$s_u=0.28$ m m,$k_0=79.0$ MPa/mm, and $G_f=0.54$N/mm. For the continue strips strengthened beams B-CS and B-CU, the parameters were as: $\tau_{\max}=3.56$ MPa,$s_0=0.046$ mm,$s_u=0.17$ mm,$k_0=77.4$ MPa/mm, and $G_f=0.30$N/mm.

Through a comparison of the three selected bond-slip constitutive relationships in this study, it is evident that the Nakaba model (Nakaba et al., 2001), which is based on in-plane shear test data, does not differentiate the influence of the spacing of FRP strips in the initial loading stage.

The Monti model (Monti et al., 2003) and Lu model (Lu et al., 2005), on the other hand, employed sophisticated finite element modeling methods. These models incorporated more influential factors such as width correction coefficient, concrete parameters, and adhesive layer parameters. Consequently, in ABAQUS, the three crucial parameters (the maximum shear stress $\tau_{\max}$, the maximum slip s_u, and the interface failure energy G_f) were employed to estimate interface damage and evolution. However, discrepancies were observed in the results based on these parameters in each model, influencing the overall interface behavior of the reinforced beams.

Furthermore, the interface behavior between FRP and concrete is notably intricate due to the variety of reinforcement forms and materials utilized in FRP shear-strengthened RC beams. As a result, using different bond-slip constitutive models to simulate these reinforced beams is a more economical and effective approach for examining the changing patterns of the interface under the influence of various factors. To assess the effectiveness and accuracy of the FRP–concrete interface bond-slip models, three representative models were employed to investigate the impact of the interface bond-slip relationship on the shear contribution of FRP based on experimental results.

3.3 Finite Element Model

In this study, the commercial finite element software ABAQUS was utilized for modeling and analysis. In this study, the commercial finite element software ABAQUS was utilized for modeling and analysis. The simulation employed three-dimensional solid elements (C3D8R) to represent the concrete, truss elements (T3D2) to model the reinforcement bars, and shell elements (S4R) to simulate the CFRP. To mitigate stress concentration during simulation, blocks were strategically positioned at the loading and support points, as depicted in Fig. 5. Moreover, the concrete damage plasticity (CDP) model available in ABAQUS was utilized to accurately simulate the behavior of the concrete material. This model accounts for the failure mechanisms associated with tensile cracking and compressive failure. The simulation incorporated user-defined uniaxial tensile and compressive relationships to characterize the yield and failure progression of the concrete. These relationships encompass linear elastic stages leading up to the failure stress, as well as softening (stretching) and hardening (compression) beyond the failure stress.

This comprehensive modeling approach facilitates an in-depth analysis of the structural response, effectively capturing the complex interactions between concrete, reinforcement bars, and CFRP. The objective of the study is to offer a thorough understanding of material behaviors and structural performance under a range of loading conditions.

In contrast to other modeling methods that disregard the bond–slip relationship between FRP and concrete by directly applying Tie constraints at the interface, this study utilized a surface-based cohesive behavior to accurately simulate the interaction. This approach employed a cohesive force contact method to connect two distinct surfaces. Notably, it only requires the input of three types of bond–slip parameters for defining the interface properties related to mutual contact.

The interface between reinforcement and concrete is appropriately simplified, and the effect of bond–slip between reinforcement and concrete is disregarded within the acceptable limits of accuracy. Embedded

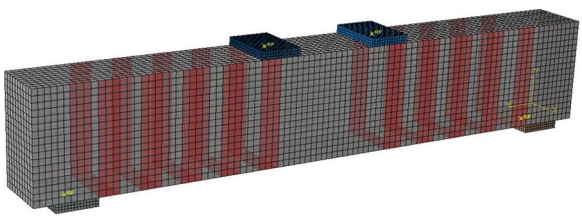

Fig. 5 Finite element modeling

constraints are employed to couple the nodes and coordinate the forces.

4 Results Analysis and Comparison

4.1 Failure Process

During the initial loading stage, cracks appeared in the pure bending section of each beam, following a similar developmental pattern across all specimens. As the load increased, numerous inclined cracks began to form in the shear span of each beam. Subsequently, a significant diagonal crack near the support progressively extended upward with continued loading. Ultimately, all test beams exhibited debonding failure of the CFRP, as depicted in Fig. 6.

The debonding process of CFRP strips in the strengthened beams progressed as follows: in comparison to the reference beams, the strengthened beams exhibited fewer cracks near the critical diagonal cracks. Following the formation of inclined cracks, the CFRP strips initially began to debond near these cracks and then progressively detached towards both the top and bottom of the beams as the load continued to increase. The peeling process continued until it reached the nearest top surface of the beam, at which point the debonding stopped until it reached the nearest top surface of the beam, at which point the debonding stopped. Simultaneously, along the direction of the inclined cracks, the entire peeling process involved the sequential detachment of CFRP strips from the initial position of the diagonal crack to the loading point.

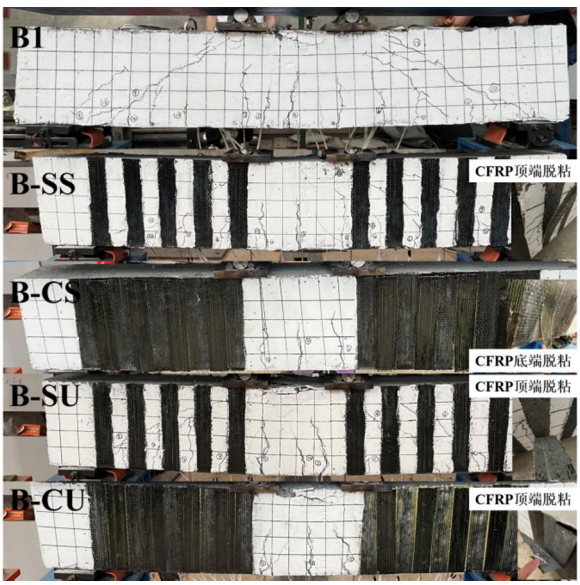

Fig. 6 Failure modes of test beams

In the finite element simulation, the failure process of the reinforced beam was characterized by five discernible stages:

Stage one: no visible cracks appeared on the surface of the specimens.

Stage two: the progression from flexural cracking to diagonal section cracking was observed. In alignment with the experimental findings, cracks initiated in the pure bending region, extending from the midspan to both ends of the beam. These cracks propagated upwards toward the top of the beam. Additionally, vertical bending cracks appeared in the shear span, altering the development pattern and resulting in the formation of numerous inclined cracks.

Stage three: as the load increased, the process of inclined cracks intersected and converged, ultimately forming a main diagonal crack at approximately a 45° angle.

Stage four: subsequent to the formation of the main diagonal crack, there was a continuous peeling of the CFRP strip.

Stage five: this stage commenced after the first strip was peeled off. As the ultimate load was reached, the crack continued to propagate and CFRP strips were successively peeled off until the beam suffered damage.

This comprehensive division of the failure process allows for a detailed understanding of the structural response, including the initiation and propagation of cracks, the formation of a main diagonal crack, and the subsequent peeling of CFRP strips leading to the ultimate failure of the beam. The simulation offers valuable insights into the behavior of the reinforced structure under a range of loading conditions, highlighting critical points of vulnerability and performance.

Figure 7 illustrates the CFRP load–strain relationship of beam B-CU in the finite element simulation with Lu's bond-slip model. The plot demonstrates that prior to the emergence of inclined cracks in the strengthened beam, the strains in the CFRP strips remained minimal. As the degree of cracking in the inclined section increased, the strains and strain growth rates of the various CFRP strips on the same strengthened beam displayed noticeable variations. The changing trends of strains at different positions highlighted the distinct paths taken by the diagonal crack, illustrating how the structural integrity of the beam is affected by the propagation of these cracks.

Table 2 provides a summary of the peeling behavior of CFRP strips in both the experimental and numerical beams. The data in the table indicate that the debonding process and characteristics of the simulated beams closely matched those observed in the test beams, particularly for the side-bonding reinforcement methods (B-SS and B-CS). However, it is important to point out

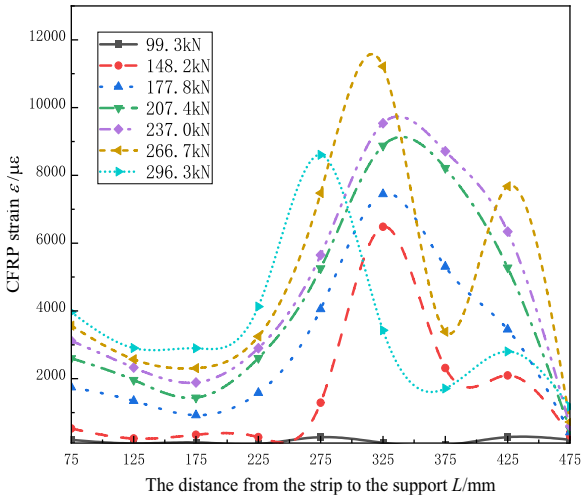

Fig. 7 CFRP load–strain relationship for B-CU beams based on Lu model

Table 2 Peeling of CFRP strips for each beam

Beams	Models	Debonding strips	Debonding load/kN
B-SS	Test	P3	241
	Nakaba	–	–
	Monti	P4,P2	210,230
	Lu	P4,P3,P2	190,230,232
B-CS	Test	P2,P5,P6	263,287,290
	Nakaba	P7,P6,P5	264,269,282
	Monti	P6,P5,P4,P3	215,215,222,270
	Lu	P6,P5,P7,P4,P3,P8	232,232,240,242,242,260
B-SU	Test	P3,P4	275,277
	Nakaba	–	–
	Mont	–	–
	Lu	P4,P3	247,274
B-CU	Test	P6,P7	310,312
	Nakaba	–	–
	Mont	P6,P7,P5	249,285,290
	Lu	P7,P6,P8	259,290,292

For the names of debonding strips, refer to Fig. 3

that only the B-CS simulated beam utilizing Lu's model interface exhibited complete peeling phenomena at the ultimate load (B-CS-Lu-P8). This discrepancy may be due to the idealized nature of the finite element simulation for concrete materials, which can lead to a higher number of cracks with locations that differ from those in actual test conditions. Additionally, the idealized interfacial failure transmission in the simulation did not accurately represent the real peeling transmission, as it is influenced by factors such as the resin adhesive's synergistic force, resulting in inconsistent peeling conditions.

For the U-jacketing methods (B-SU and B-CU), the Nakaba model failed to simulate the debonding of the strips. In contrast, the ultimate strain of the debonded strips in the other two models (Monti and Lu models) was greater than that observed in beams strengthened by side-bonding methods, which is consistent with the experimental findings. Additionally, unlike CFRP discrete reinforcement, CFRP continuous reinforcement resulted in adjacent strips being bonded together with resin glue, enhancing their cohesive performance.

Consequently, gradual peeling under load frequently occurred in several adjacent strips. When one strip was peeled off, the residual adhesive on that strip continued to provide support to the adjacent strips, transferring load through the resin glue. This interaction contributed to a larger ultimate strain for CFRP under continuous reinforcement. Consequently, the U-shaped and continuous reinforcement methods demonstrated more effective reinforcement performance for the materials.

4.2 Effect of Strengthening

Table 3 presents the characteristic loads of the five test beams obtained from both experimental and finite element methods. Notably, when the first crack appeared in the pure bending section of the strengthened beams, there was minimal disparity in the loads. This similarity can be attributed to the limited effectiveness of the CFRP strips prior to the development of inclined cracks, as they were unable to significantly hinder crack propagation. During this phase, the concrete predominantly provided shear resistance, leading to an overall similar cracking load for both the normal and inclined sections across all test beams.

In the experiment, the four shear strengthening methods exhibited an enhancement in ultimate load ranging from 13.5% to 42.9%. The U-jacketing strengthening configuration notably outperformed the side strengthening method, with a 13.9% increase in ultimate load between B-SS and B-SU, and a 10.8% increase between B-CS and B-CU. Additionally, the center distance of CFRP strips played a role in influencing the ultimate load. For instance, B-CS achieved an 18.6% higher load than B-SS, and B-CU exhibited a 15.5% higher load than B-SU, respectively.

Comparing the ultimate loads obtained through the finite element method with experimental values revealed generally good agreement. With the exception of B-SU-Monti (with a relative error of −14.1%), all other errors were below 7.1%. Similarly, with the exception of the limit displacement B-CU-Lu (with a relative error of −14.2%), all other errors were below 10.7%. Considering factors such as the divergence between actual tests and loading processes, measurement errors, and the inherent

Table 3 Characteristic load and failure model of beams

Beam	Model	P_{cr}^{b}	P_{cr}^{s}	P_u	Increase of P_u	Error of P_u	d_u	Error of d_u
B1	Test	35.1	85.1	219.9	–	–	5.40	–
	FEA	63.9	91.7	231.2	–	5.1	5.25	-2.70
B-SS	Test	47.0	112.8	249.5	13.5	–	4.40	–
	Nakaba	67.4	93.5	260.2	18.3	4.3	4.42	−1.10
	Monti	64.8	94.1	232.0	5.5	−7.0	4.49	0.44
	Lu	66.5	93.5	242.6	10.3	−2.8	4.41	−1.30
B-CS	Test	52.5	–	290.5	32.1	–	4.00	–
	Nakaba	67.7	95.1	299.9	36.4	3.2	4.30	7.50
	Mont	68.1	92.1	270.1	22.8	−7.0	3.96	−1.00
	Lu	69.3	95.3	269.8	22.7	−7.1	3.57	−10.70
B-SU	Test	50.0	103.7	280.2	27.4	–	4.00	–
	Nakaba	72.7	102.2	286.6	30.3	2.3	3.79	−5.20
	Monti	70.8	102.1	240.8	9.5	−14.1	3.59	−10.20
	Lu	71.4	100.3	275.1	25.1	−1.8	3.79	−5.20
B-CU	Test	53.7	–	314.3	42.9	–	3.50	–
	Nakaba	72.1	110.1	324.9	47.7	3.4	3.68	5.10
	Monti	68.6	103.3	292.4	32.9	−6.9	3.58	2.20
	Lu	72.7	99.3	296.3	34.7	−5.7	3.00	−14.20

P_{cr}^{b} is the bending cracking load, P_{cr}^{s} is the shearing cracking load, P_u is the ultimate load, 'Error of P_u' respresents the relative error between analysis and test results of P_u,d_u is the displacement at ultimate load, 'Error of d_u' respresents the relative error between analysis and test results of d_u, load unit: 'kN', deflection unit: 'mm', error unit: '%'

variability of concrete, it is deemed that the simulation errors for each model were within an acceptable range.

Furthermore, an analysis of the data in Table 3 revealed discrepancies in ultimate loads and displacements when simulating three different bond-slip relationships for the same beam. These divergences can be attributed to variations in the definitions regarding the initiation of the bond interface's entry into the softening stage, the progression of interface failure, and the evolution of stress and damage. Consequently, these differences resulted in distinct calculation outcomes for each simulation scenario.

4.3 Load–Deflection Behavior

Figure 8 illustrates a comprehensive comparison of the load–displacement relationships derived from the finite element simulations of five beams, incorporating three distinct bond-slip relationships, against the corresponding experimental results. The graphical representation reveals that, during the initial loading phase prior to concrete cracking, the slope of the finite element model's curve is slightly steeper than that of the experimental curve. As the applied load increases, the curve slope progressively converges towards the experimental values, demonstrating a consistent and steady progression towards alignment with the observed experimental behavior.

Upon closer examination, it is evident that the load–displacement curve from the finite element simulation demonstrates strong alignment with the experimental curve overall. The discrepancies observed in the initial loading stage are mitigated as the load increases, resulting in a convergence of the two curves. This observation indicates a robust agreement between the finite element model and the experimental outcomes, thereby affirming the credibility and accuracy of the simulation in capturing the structural behavior across various bond-slip relationships.

4.4 Interface Failure Process

To fully comprehend the impact of the bond-slip relationship on the interface of CFRP-strengthened beams, it is essential to analyze the failure process of the FRP–concrete interface. The development and failure process of CFRP shear-strengthened beams can be categorized into four distinct stages. Figure 9 illustrates the distribution nephogram of interface failure for B-SS beams across these four stages of loading.

In the first stage of interface failure, prior to the emergence of the primary diagonal crack, there was minimal failure observed. During this period, the CFRP strips remained unstressed, which resulted in no significant changes in shear force or displacement within the interface. As inclined shear cracks developed, the interface

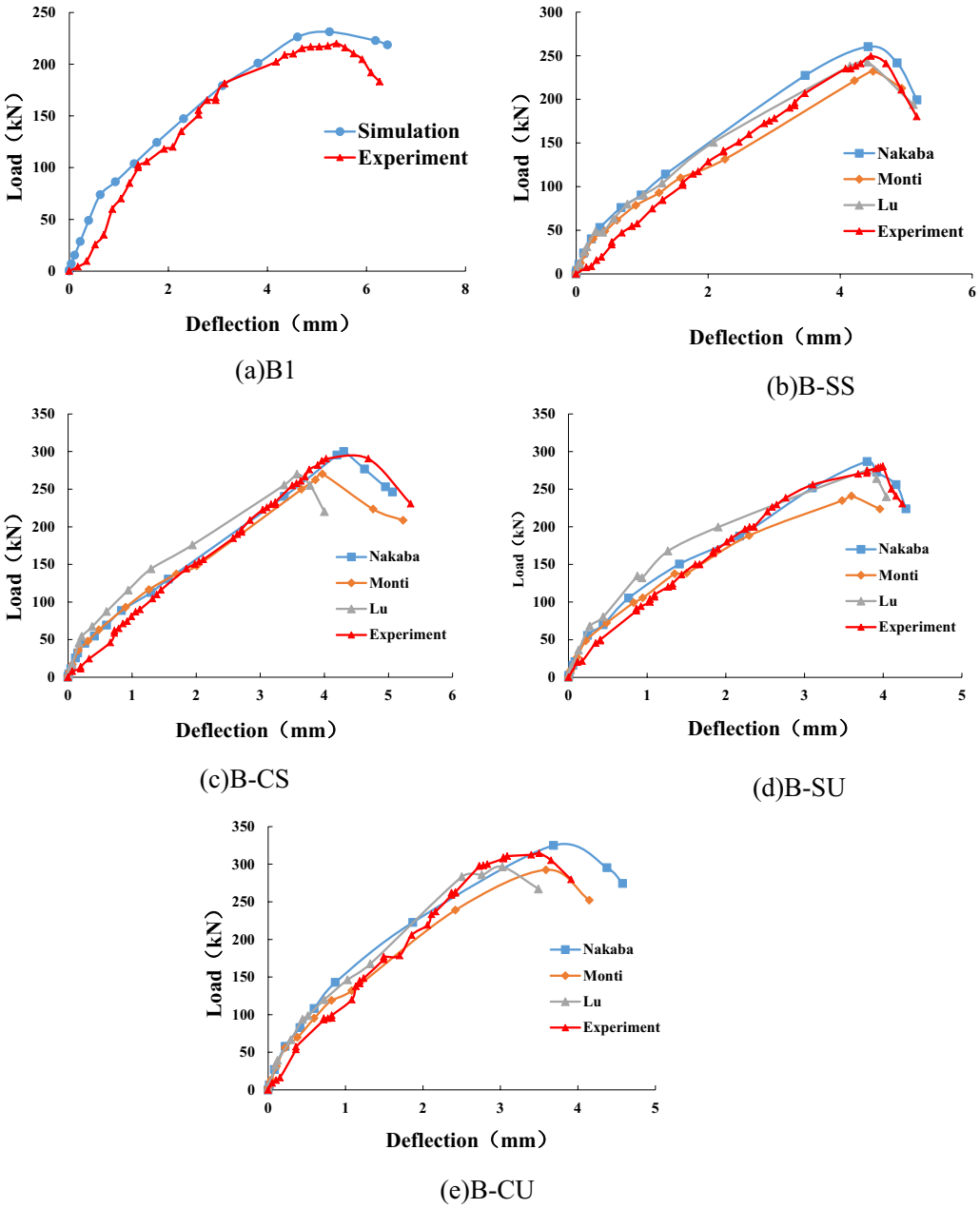

Fig. 8 The load–deflection curve of all test beams

failure progressed to the second stage. In the early phase of this stage, the CFRP experienced a slight strain; however, the mechanical characteristics of the interface remained largely unchanged. The shear force and slip within the interface displayed minor fluctuations, while the interface nephogram began to reveal the progression of damage. This trend continued until reaching the second interface failure load, with the values for the three bond-slip models of the B-SS beams recorded as 106.1 kN, 100.9 kN, and 102.7 kN, respectively. The initial position of damage evolution was near the bottom of P3 and the middle of the P4 strip, corresponding to the generation of inclined cracks.

In the third stage, an inclined crack began to propagate across the CFRP strips, progressively extending toward both the loading point and the support position. At this stage, debonding of the concrete–FRP interface initiated, initially moving upward and downward along the beam. This process of debonding persisted until the applied load reached the third interface failure load, with

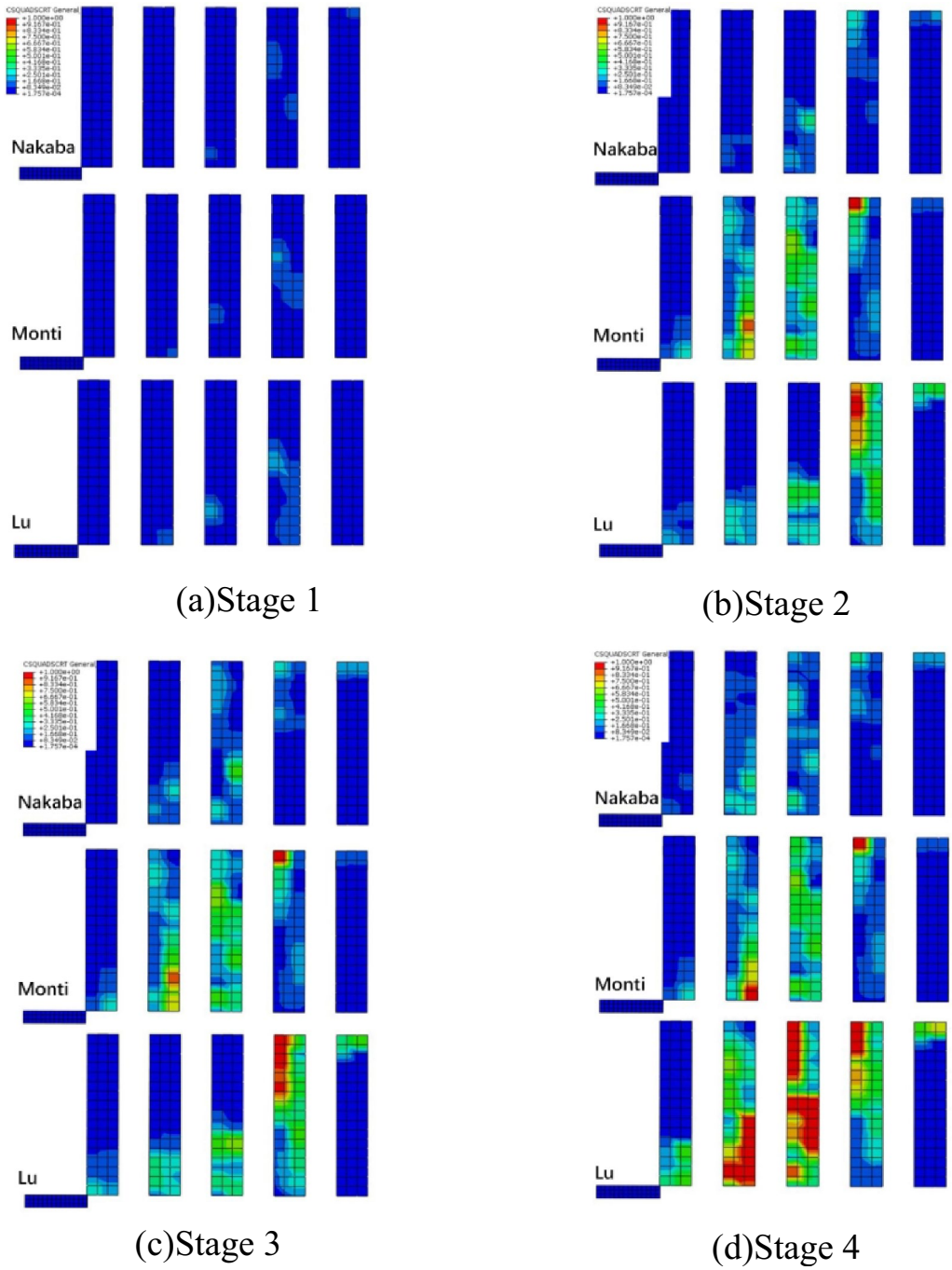

Fig. 9 Interface failure distribution at each stage of B-SS beam

the respective values for the two bond-slip models of the B-SS beams recorded as 210.2 kN and 182.6 kN.

In the final stage, as the load increased to the interface failure load 4 (with a value of 190.0 kN for the B-SS-Lu model), the interface failure continued, propagating both upward and downward along the depth of the beam from the initial debonding site. The interface slip escalated rapidly at the location where the diagonal crack intersected, extending to the nearest point on the beam's top. Ultimately, the bond became inadequate to sustain the shear force, causing the beam to reach the interface failure load 5 (the ultimate load).

Figures 10 and 11 illustrate the distribution of shear forces and slip for the B-SS-Monti P4 and B-SS-Lu P4 strips along the beam depth, both before and after the interface failure load in the third stage. At the debonding site, the interfacial shear force and slip values approached their ultimate levels just before debonding took place, reaching 6.97 MPa and 0.4 mm in the Monti model, and 4.74 MPa and 0.28 mm in the Lu model, respectively. In this scenario, the slip at positions distant from the debonding point was less than 0.2 mm. Once the shear force at the interface reached the damage criterion, the shear force at the debonding interface plummeted to 0, and the corresponding interface slip instantaneously exceeded the ultimate slip value. The shear strength swiftly transferred to the nearest point in the height direction of the strips, resulting in a minor change in shear force at the nearby interface.

4.5 Shear Contribution of CFRP Based on Bond–Slip Model

Table 4 provides a comparison between the simulated contribution values of FRP shear capacity based on different interface bond-slip models and the experimental values. It is evident that the simulation results from the Nakaba interface model for the four reinforced beams were consistently higher, with an average ratio of the simulated value to the experimental value of FRP shear capacity being 1.18.

This discrepancy can be attributed to the Nakaba model's failure to distinguish between discrete and continuous reinforcement when compared to the other two models. Specifically, the model did not consider the influence of the width correction coefficient on the interface bond-slip curve. Consequently, the three crucial parameters used for assessing interface damage and evolution in the ABAQUS software were the largest among the three bond-slip models. This characteristic rendered the

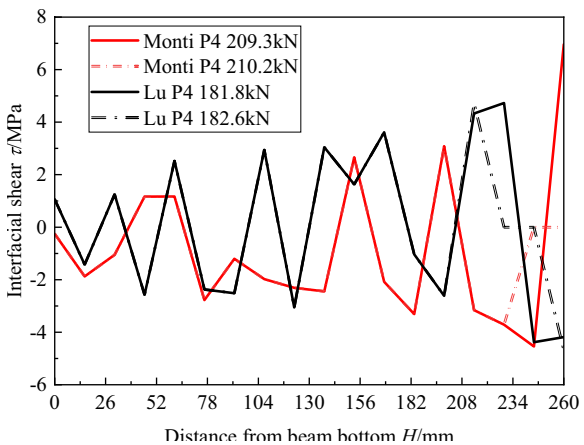

Fig. 10 Interfacial shear force along beam height during debonding

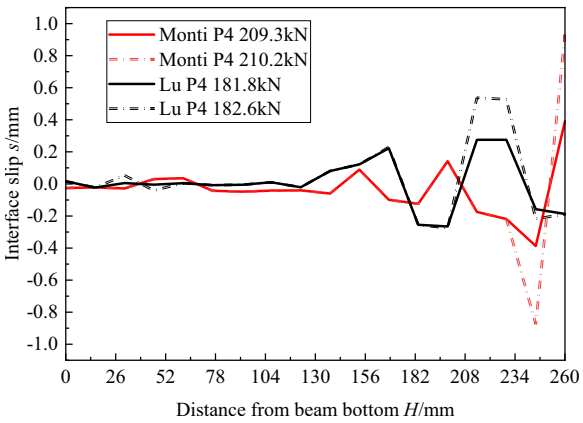

Fig. 11 Interface slip along beam height during debonding

FRP–concrete interface simulated by the Nakaba model less prone to debonding, resulting in a slower progression of interface damage.

Although the FRP shear contribution and the load–deflection change of the Nakaba model demonstrated better agreement with the experimental tests, the simulation effectiveness of the U-jacket and discrete reinforcement was not as robust as that of the other two models. This observation stems from the behavior of FRP strip

Table 4 Comparison of finite element and experimental shear contributions of CFRP

Beams	B-S models	P_u/kN	V_f/kN	V_{fs}/V_{tf}
B1	Test	219.9	—	—
	FEA	231.2	—	—
B-SS	Test	249.5	29.6	—
	Nakaba	260.2	40.3	1.36
	Monti	232.0	12.1	0.41
	Lu	242.6	22.7	0.77
B-CS	Test	290.5	70.6	—
	Nakaba	299.9	80.0	1.13
	Monti	270.1	50.2	0.71
	Lu	269.8	49.9	0.71
B-SU	Test	280.2	60.3	—
	Nakaba	286.6	66.7	1.11
	Monti	240.8	20.9	0.35
	Lu	275.1	55.2	0.92
B-CU	Test	314.3	94.4	—
	Nakaba	324.9	105.0	1.11
	Monti	292.4	72.5	0.77
	Lu	296.3	76.4	0.81
Average	Nakaba		1.18	
	Monti		0.56	
	Lu		0.80	

debonding and the progression of interface damage, as discussed in the previous section.

The simulated results from both the Monti and Lu models were consistently lower than the experimental values, with average ratios of the simulated values to experimental values being 0.56 and 0.80, respectively. Regarding the shear contribution by these two models, the U-jacket reinforcement mode demonstrated a closer alignment with the experimental values compared to the side-bonded reinforcement mode. Additionally, the continuous reinforcement mode was found to be more consistent with the experimental results than the interval reinforcement mode. Upon comparing the three critical parameters of the Monti model and Lu model under discrete and continuous strengthening, it was observed that the maximum shear stress, maximum slip, and maximum fracture energy of the Monti model were all greater than those of the corresponding Lu model. This suggests that the shear contribution of CFRP in the Monti model should be more significant than that in the Lu model. However, a closer examination of the interface damage process of B-SS beam and B-SU beam, the CFRP stress diagram, crack trench diagram under ultimate load, and the load–deflection curve reveals that although the strip stress of the Monti model was greater than that of the Lu model as the beam approached the ultimate load, the interface damage was not as extensive as in the Lu model. Specifically, the critical diagonal crack width of the Monti model under the same load exceeded that of the Lu model, and the position of the inclined crack was closer to the top of the beam. This observation is further supported by the crack diagram observed under the ultimate load in the test results. Although the Monti model provides a greater bond length than the Lu model, the overall stiffness of the beam in the Monti model decreased more rapidly. This led to a lower shear contribution compared to the Lu model.

5 Conclusions

In this study, a control beam and four strengthened beams with varying shear reinforcement configurations were tested to assess the improvement in shear capacity. Furthermore, all test beams were simulated using the finite element software ABAQUS, which included three different bond-slip relationships for the FRP–concrete interface for each strengthened beam. The analysis of the test and simulation results led to the following conclusions:

1 The overall simulation results of the load–displacement curve exhibit a high level of agreement with the experimental curve, with numerical errors for the ultimate load and the corresponding deflection ranging from -14.1% to 7.5%.
2 Among all the strengthened beams, the continuous configuration demonstrates a superior effect compared to the discrete configuration, while U-jacketed reinforcement is found to be more effective than side-bonding reinforcement. During the experimental phase, the shear capacity of the four types of reinforcement increased by 13.5% to 42.9%. The finite element simulations indicated that the shear capacity increased by 5.5% to 47.7%. Additionally, the shear contribution of CFRP for the four reinforcement types ranged from 12.1 kN to 105.0 kN.
3 Before the formation of the main diagonal crack, the FRP strips used in the four strengthening methods have minimal influence on shear resistance, with the shear force primarily supported by the concrete. Once the diagonal crack appears, the FRP strips begin to counteract crack propagation and actively contribute to shear resistance. Both the continuous and U-jacketed strengthening configurations demonstrate the ability to fully leverage the shear-strengthening capabilities of CFRP, effectively utilizing its tensile strength.
4 Prior to the failure of the interface of the FRP shear-strengthened concrete beam, the interface shear force and slip quickly reach and exceed the limit dictated by the corresponding bond-slip relationship. Following this, debonding begins at the initially damaged interface and propagates into the surrounding area. This debonding process plays a crucial role in the overall debonding and peeling of the FRP strip.
5 For FRP–concrete interface failure in shear-strengthened beams, three different bond-slip relationships simulate different degrees of interface degradation and failure. The larger the three critical parameters in the bond-slip model, the more difficult it is for the interface to fail, resulting in a higher shear contribution from the FRP. However, changes in these parameters also affect the propagation of interface failure and alter the flow of the finite element simulation beams. In addition, these changes affect the peeling behavior, crack propagation and ultimate load capacity of the FRP. The definition of the accurate bond-slip relationship is crucial as it significantly affects the performance of the bond interface of FRP concrete and consequently the shear contribution of the FRP.

Acknowledgements
The authors would like to thank the Natural Science Foundation of Xinjiang Uygur Autonomous [2020D01C027]. The authors are grateful for the support.

Author contributions
SQ Ma: supervised the student, prepared the research plan, shared in the theoretical work, and participated in writing and reviewing the article. JF Sun: wrote the article, carried out the experimental work, shared in the theoretical work and shared in the final revision. TC Xu: carried out the experimental work and revised the final revision. All authors read and approved the final manuscript.

Funding
Open access funding supported by the Fundamental Research Funds for the Central Universities, CHD300102219525 and Xinjiang Key R&D Program Projects (grant numbers 2022B03033-1) and the Xinjiang Uygur Autonomous Region 'Dr. Tianchi' Project.

Availability of data and materials
All data generated or analyzed during this study are included in this published article.

Declarations

Competing interests
No competing interests exit in the submission of this manuscript, and the manuscript is approved by all authors for publication. The author declares that the work described was original research that has not been published previously, and not under consideration for publication elsewhere, in whole or in part.

Received: 28 December 2023 Accepted: 17 September 2024
Published online: 09 January 2025

References

Askar RaA, Abd-Alkhalek M. (2012). Response of RC box girders strengthened using cfrp sheets. *Journal of American Science, 8*(12).
Beber A, Campos Filho A. (2005). CFRP composites on the shear strengthening of reinforced concrete beams. *Revista IBRACON de Estruturas, 1*(2).
Chaallal, O., Nollet, M.-J., & Perraton, D. (1998). Shear strengthening of RC beams by externally bonded side CFRP strips. *Journal of Composites for Construction, 2*(2), 111–113.
Chen, J., & Teng, J. (2003). Shear capacity of FRP-strengthened RC beams: FRP debonding. *Construction and Building Materials, 17*(1), 27–41.
China TDOTPSRO. Specifications for Design of Highway Reinforced Concrete and Prestressed Concrete Bridges and Culverts (JTG 3362–2018).
Ding, F. X., Ying, X. Y., & Yu, Z. W. (2010). Unified calculation method of uniaxial mechanical properties of lightweight aggregate concrete. *Journal of Central South University (Science and Technology), 41*(5), 1973–1979.
Ding, F. X., Ying, X. Y., Zhou, L. C., & Yu, Z. W. (2011). Unified calculation method and its application in determining the uniaxial mechanical properties of concrete. *Frontiers of Architecture and Civil Engineering in China, 5*(3), 381–393. https://doi.org/10.1007/s11709-011-0118-6
Dong, J., Wang, Q., & Guan, Z. (2013). Structural behaviour of RC beams with external flexural and flexural–shear strengthening by FRP sheets. *Composites Part B: Engineering, 44*(1), 604–612. https://doi.org/10.1016/j.compositesb.2012.02.018
Haddad, R. H., Al-Rousan, R. Z., & Al-Sedyiri, B. K. (2013). Repair of shear-deficient and sulfate-damaged reinforced concrete beams using FRP composites. *Engineering Structures, 56*, 228–238. https://doi.org/10.1016/j.engstruct.2013.05.007
Islam, M. R., Mansur, M. A., & Maalej, M. (2005). Shear strengthening of RC deep beams using externally bonded FRP systems. *Cement and Concrete Composites, 27*(3), 413–420. https://doi.org/10.1016/j.cemconcomp.2004.04.002
Jahangir, H., & Esfahani, M. R. (2018). Numerical study of bond – slip mechanism in advanced externally bonded strengthening composites. *KSCE Journal of Civil Engineering, 22*(11), 4509–4518. https://doi.org/10.1007/s12205-018-1662-6
JTG 3362–2018, Specifications for design of highway reinforced concrete and prestressed concrete bridges and culverts.
Khalifa, A., & Nanni, A. (2000). Improving shear capacity of existing RC T-section beams using CFRP composites. *Cement and Concrete Composites, 22*(3), 165–174. https://doi.org/10.1016/S0958-9465(99)00051-7
Lee, T. K., & Al-Mahaidi, R. (2008). An experimental investigation on shear behaviour of RC T-beams strengthened with CFRP using photogrammetry. *Composite Structures, 82*(2), 185–193. https://doi.org/10.1016/j.compstruct.2006.12.012
Lee, D. H., Han, S.-J., Kim, K. S., et al. (2017). Shear strength of reinforced concrete beams strengthened in shear using externally-bonded FRP composites. *Composite Structures, 173*, 177–187. https://doi.org/10.1016/j.compstruct.2017.04.025
Li, K., Cao, S., Yang, Y., et al. (2018). Bond-slip relationship for CFRP sheets externally bonded to concrete under cyclic loading. *Materials, 11*(3), 336.
Lin, X., & Zhang, Y. X. (2013). Bond–slip behaviour of FRP-reinforced concrete beams. *Construction and Building Materials, 44*, 110–117. https://doi.org/10.1016/j.conbuildmat.2013.03.023
Lu, X. Z., Teng, J. G., Ye, L. P., et al. (2005). Bond–slip models for FRP sheets/plates bonded to concrete. *Engineering Structures, 27*(6), 920–937. https://doi.org/10.1016/j.engstruct.2005.01.014
Ma, S., Muhamad Bunnori, N., Choong, K. K., et al. (2019). Models reviewed for predicting CFRP shear contribution of strengthened reinforced concrete box beam. *KSCE Journal of Civil Engineering, 23*(8), 3644–3659. https://doi.org/10.1007/s12205-019-1850-z
Monti G, Renzelli M, Luciani P. (2003). *FRP adhesion in uncracked and cracked concrete zones*.
Moradi, E., Naderpour, H., & Kheyroddin, A. (2020). An experimental approach for shear strengthening of RC beams using a proposed technique by embedded through-section FRP sheets. *Composite Structures, 238*, 111988. https://doi.org/10.1016/j.compstruct.2020.111988
Nakaba, K., Kanakubo, T., Furuta, T., & Hiroyuki, Y. (2001). Bond behavior between fiber-reinforced polymer laminates and concrete. *ACI Structural Journal*. https://doi.org/10.14359/10224
Nelson, A. L., Al-Allaf, M., & Weekes, L. (2020). Analytical modelling of bond-slip failure between epoxy bonded FRP and concrete substrate. *Composite Structures*. https://doi.org/10.1016/j.compstruct.2020.112596
Panigrahi, A. K., Biswal, K., & Barik, M. (2014). Strengthening of shear deficient RC T-beams with externally bonded GFRP sheets. *Construction and Building Materials, 57*, 81–91.
Pellegrino, C., & Modena, C. (2006). Fiber-reinforced polymer shear strengthening of reinforced concrete beams: experimental study and analytical modeling. *ACI Structural Journal, 103*(5), 720.
Pellegrino, C., & Modena, C. (2008). An experimentally based analytical model for the shear capacity of FRP-strengthened reinforced concrete beams. *Mechanics of Composite Materials, 44*(3), 231–244.
Sayed, A. M., & Wang, XWu. Z. (2014). Finite element modeling of the shear capacity of RC beams strengthened with FRP sheets by considering different failure modes. *Construction and Building Materials, 59*, 169–179. https://doi.org/10.1016/j.conbuildmat.2014.02.044
Teng, J. G., Chen, J. F., Smith, S. T., et al. (2003). Behaviour and strength of FRP-strengthened RC structures: A state-of-the-art review. *Proceedings of the Institution of Civil Engineers - Structures and Buildings, 156*(1), 51–62. https://doi.org/10.1680/stbu.2003.156.1.51
Triantafillou, T. C., & Plevris, N. (1992). Strengthening of RC beams with epoxy-bonded fibre-composite materials. *Materials and Structures, 25*(4), 201–211. https://doi.org/10.1007/BF02473064
Zhi-Wu, Y. (2010). Unified calculation method of uniaxial mechanical properties of lightweight aggregate concrete. *Journal of Central South University, 41*(5), 1937.
Zhou, Y., Guo, M., Sui, L., et al. (2019). Shear strength components of adjustable hybrid bonded CFRP shear-strengthened RC beams. *Composites Part b: Engineering, 163*, 36–51. https://doi.org/10.1016/j.compositesb.2018.11.020

Publisher's Note

Shengqiang Ma Associate professor, PhD, College of Architectural and Civil Engineering, Xinjiang University, Urumqi, 830049, China. Major in bridge engineering.

Jianfeng Sun Graduate student, College of Architectural and Civil Engineering, Xinjiang University, Urumqi, 830049, China.

Tiancai Xu Graduate student, College of Architectural and Civil Engineering, Xinjiang University, Urumqi, 830049, China.